P-52

Star Formation and the Distribution of HI and Infrared Emission in M51

Richard J. Rand and Shrinivas R. Kulkarni[1]

California Institute of Technology

and

W. Rice

Infrared Processing and Analysis Center,

Jet Propulsion Laboratory,

California Institute of Technology

[1] Alfred P. Sloan Fellow and Presidential Young Investigator

Abstract

HI, infrared, CO, Hα and B-band observations of M51, the prototypical grand-design spiral galaxy, are used to study the consequences of star formation for the distribution of HI and dust. Using the HI and CO data sets we carry out new tests of the idea of Tilanus and Allen that the HI is largely a dissociation product in star-forming regions. We confirm that the HI spiral arms are generally coincident with the HII region arms, and offset downstream from the CO arms. The radial distributions of total gas, Hα and HI surface density have a simple explanation in the dissociation picture. The distributions also demonstrate how the surface density of HI might be related to the star formation efficiency in molecule-rich galaxies. The large width of the HI regions along the arms compared to that of the HII regions can be understood in terms of a simple "Strömgren sphere" calculation. The longer lifetime of the stars producing dissociating radiation $vs.$ those producing ionizing radiation will also contribute to the greater width of the HI arms if stars are continuously forming on the arms. The lack of detailed coincidence of the HI and HII regions along the inner arms has a variety of possible explanations within the dissociation scenario.

We carry out two simple tests to probe the origins of the $IRAS$ emission in M51. First, we find that the infrared excess (IRE) of M51 is 24, suggesting that a substantial fraction of the infrared emission arises from dust outside of star-forming regions. Second, radial cuts through the $IRAS$ bands show that at 12,

25 and 60 μm, the arm-interarm contrast of the *IRAS* emission is substantially less than that of the Hα emission, convolved to matching resolutions, providing further evidence that there are large amounts of dust not associated with star-forming regions. Deconvolved *IRAS* maps have improved resolution but do not change the above finding.

Subject headings: galaxies: interstellar matter – galaxies: individual (M51) – stars: formation – infrared: sources

I. Introduction

Great advances in our understanding of how spiral density waves organize atomic and molecular gas in galaxies and how they therefore relate to ongoing star formation have been made possible in the past few years with the advent of high-resolution centimeter- and millimeter-wave interferometers. M51 has been a popular target for such studies because of its proximity (9.6 Mpc; Sandage and Tammann 1975), nearly face-on aspect, strong spiral structure, and molecule-rich ISM (about 90% of the ISM is molecular; Scoville and Young 1983). Observations of the ISM of this galaxy have been recently reviewed by Rand and Tilanus (1990).

In two previous papers (Vogel, Kulkarni, and Scoville 1988, hereafter VKS; Rand and Kulkarni 1990a, hereafter RK) we have presented mosaic maps of CO $1 - 0$ emission from M51 at 8" resolution made with the Millimeter Interferometer of the Owens Valley Radio Observatory (OVRO). We detected molecular spiral arms which are well aligned with the dust lanes but offset upstream from the HII region arms (see Figure 1a,b), implying that the onset of massive star formation occurs several million years after the peak compression of the molecular gas. The spiral arms represent about one-third of the total emission measured with single dish instruments. The tangential and radial velocity shifts predicted by density wave theory as the gas is being compressed can be clearly seen where the arms cross the major and minor axes of the galaxy. Using Hα emission as a tracer of the massive star formation rate, we found that the star formation efficiency is higher on the arms than between the arms, implying that the density wave is triggering

excess star formation from the compressed gas. This result has been confirmed in single-dish CO observations (Lord and Young 1990). The molecular arms contain well-organized structures which we termed Giant Molecular Associations (GMAs). The typical mass of a GMA is 3×10^7 $M_\odot$. GMAs are also found between the arms. The on-arm GMAs are roughly gravitationally bound, while the interarm GMAs are unbound. The CO 1–0 spectra of the GMAs show that they typically consist of one to five velocity components. The GMAs may form through collisional agglomerations of pre-existing smaller clouds or by gravitational instabilities in the molecular gas (see Rand and Kulkarni 1990b). The interarm GMAs may owe their existence to a weak, secondary compression of the density wave.

VKS and RK examined how the density wave organizes the molecular gas and discussed the consequences for star formation from analysis of Hα images. In this paper, we further examine the "back reaction" of star formation on the ISM of M51 by considering, in conjunction with molecular data, the distribution of atomic gas and infrared emission from two new data sets: the VLA map of 21-cm emission by Rots et al. (1990, hereafter RBHAC), and the IRAS (Infrared Astronomical Satellite) pointed observations of M51 (Rice et al. 1988).

Recently, evidence has been presented that in the molecule-rich galaxies M51 (Tilanus and Allen 1989, hereafter TA) and M83 (Allen, Atherton, and Tilanus 1986) HI is predominantly a product of dissociation of H$_2$ in star-forming regions. If the detected HI were distributed in the same way as all the gas we would expect to see the peak of the 21-cm emission along the dust lanes, where the highest compression

of the gas is occurring. However, the observations show that in these galaxies HI is concentrated downstream from the dust lanes but coincident with the HII region arms. TA estimate that in M51 approximately 10% of the molecular gas is dissociated in star-forming regions. Compared to the WSRT map of TA, the new VLA 21-cm emission map of M51 by RBHAC has higher resolution (8" vs. 12" x 18") and sensitivity. In this paper we use this map, along with our Hα and B-band images, CO data (see RK) and the single-dish CO data of Lord and Young (1990) to carry out further quantitative tests of the dissociation scenario. In particular, we examine whether a) the radial distributions of total gas, Hα and HI, b) the small-scale structure of the HI emission and c) the detailed spatial relationship between the HI and HII regions can be explained in this picture. We find that the new VLA map provides further evidence in favor of the dissociation scenario.

Radiation from young stars not only ionizes HI and dissociates H$_2$ but also heats the interstellar dust. The infrared emission from dust allows yet another probe of the back reaction of star formation on the ISM. In the second part of this paper, we use the *IRAS* pointed observations of M51 to study the distribution and origins of the infrared emission. Recent work on the *IRAS* spectra of our Galaxy and other spirals (Cox and Mezger 1987; Lonsdale-Persson and Helou 1987; Helou 1986) has led to a picture for the dust emission in which the 12 μm emission is dominated by very small grains transiently heated by the interstellar radiation field (ISRF; there may also be a contribution from OH/IR stars), the 25 and 60 μm emission is from warm dust in star-forming regions but may also have a substantial contribution from generally distributed dust heated by the ISRF, and the 100 μm emission is

dominated by relatively large grains heated by the ISRF. The very small grains are expected to be destroyed in star-forming regions (Puget, Léger, and Boulanger 1985), so little 12 μm emission is expected from such regions. Broadly distributed dust heated by the ISRF has come to be referred to as "cirrus" (Low *et al.* 1984).

We attempt to interpret the infrared emission of M51 in terms of these two components: dust in star-forming regions and cirrus. Our goal is to understand the origins of the *IRAS* emission in M51. In particular, we carry out two tests designed to distinguish between infrared emission arising from star-forming regions, and emission from a cirrus component. We first calculate the "Infrared Excess" (IRE; Mezger 1978), a dimensionless quantity which provides a measure of the fraction of the infrared flux which arises from star-forming regions. We then compare cuts through the *IRAS* maps with cuts through Hα and *B*-band CCD images convolved to the *IRAS* resolutions to determine whether the infrared emission is distributed in the same way as the optical line emission from star-forming regions. If the infrared emission shows a reduced concentration to the spiral arms compared to the Hα emission, then one can conclude that a fraction of the infrared emission arises from generally distributed dust. We find that the results of both these tests indicate that a substantial fraction of the emission detected by *IRAS* does not originate in star-forming regions.

II. HI and Dissociation

a). Radial Distributions

The radial distributions of the total gas, $H\alpha$ and HI surface density are shown in Figure 2. To estimate the total (H_2 and HI) gas surface density, we have used the FCRAO map of CO emission at 45" resolution by Lord and Young (1990). To convert the CO emission to molecular column density, we assume the Galactic conversion factor of $\alpha = 3 \times 10^{20}$ mol cm^{-2} (K km s^{-1})$^{-1}$. The FCRAO map is used here and below whenever complete information on the molecular gas surface density is required. The total gas profile shows a roughly exponential fall-off with radius, while the $H\alpha$ profile shows a similar fall-off, but with a pronounced enhancement at $R \approx 150"$. The HI profile shows a central hole ($R \lesssim 30"$), a relatively flat inner disk ($30" \lesssim R \lesssim 100"$), a large enhancement in the outer disk peaking at $R \approx 150"$, and finally a falloff at $R \gtrsim 175"$. This profile can be understood in terms of the theory of Federman, Glassgold, and Kwan (1979), who consider the shielding of a molecular cloud to dissociating radiation by an outer envelope of HI. In this picture, the thickness of the dissociated envelope depends on the ratio of the dissociation and formation rates of H_2. This ratio has been shown by Hollenbach, Werner and Salpeter (1971) to depend on a power of G/n, where G is essentially the flux of dissociating radiation times the cross section in the Lyman bands of H_2, and n is the density of the gas. Here we are considering the creation of dissociated envelopes in star-forming regions by energetic photons from the young stellar associations. Since $H\alpha$ traces the high-mass stars it should also trace the dissociating radiation. The flat HI profile in the inner disk and the large enhancement in HI around $R \approx 150"$ can then be understood in terms of this simple balance between molecule formation and dissociation in star-forming regions. In the inner disk at $R \lesssim 100"$, the $H\alpha$

and total gas profiles show a similar falloff with radius, so that the balance between dissociation and formation changes little with radius and a constant column density of HI is produced. At $R \approx 150"$, the "excess" of dissociating radiation in the outer arms relative to the gas density tips the scales in favor of dissociation, and thus more HI is produced. Beyond $R = 170"$, the $H\alpha$ enhancement ends, and the HI returns to roughly its inner disk value. The radial distributions therefore support the dissociation picture.

An interesting consequence of such an interpretation for the origin of the HI is that, since the $H\alpha$ emission traces the star formation rate, the HI surface density is actually related to the star formation *efficiency* (the star formation rate per unit gas mass). The possibility of using HI as an indicator of star formation efficiency in molecule-rich galaxies such as M51 and M83 should be pursued further.

b). The Small-scale Structure

In Figure 1c,d we show the VLA HI map of RBHAC overlaid on our CO map and $H\alpha$ image. It is clear that compared to the CO distribution there is enhanced HI emission in the outer ($R \gtrsim 100"$) arms, although the azimuthally averaged column density of HI rises to a peak of only 40% of that of H_2 as determined from the FCRAO CO map (the units of the H_2 column density are atoms cm^{-2}). Comparing with the OVRO CO map, we find a typical ratio of H_2 to HI column density in the inner arms of about 16. Therefore the new VLA map confirms the low HI/H_2 ratio on the arms, and the conclusion of TA that only a small fraction of the molecular gas is dissociated.

From the VLA HI map (Figures 1c,d) we note the following:

i) Over large sections of the inner ($R \lesssim 100''$) arms (see Figure 1c) an offset can be seen between the centroids of the HI arms and CO arms, but the broad HI emission in many places extends upstream to the CO arms and often even *further* upstream into the pre-compression zone.

ii) The inner HI arms show a patchy structure and are broader than the Hα arms. The typical diameter (FWHM) of the bright HII regions in the inner arms is 5.5'' or 250 pc, while the typical diameter of the HI arms is about 17'' or 800 pc, although there is much variation in the latter quantity.

iii) While parts of the inner arms show a simple morphology in which HI envelopes exist around HII regions, there are many HI clouds which have very little Hα emission associated with them, as in M83 (Allen, Atherton, and Tilanus 1986). Figure 3 is a close-up view of an arm segment which shows the detailed spatial correspondence of the CO, 21-cm, and Hα emission.

iv) There are a few HI clouds in the interarm regions, where there is also very little or no Hα emission. It should be pointed out that the total mass of HI in the VLA 8''-resolution map is 2×10^9 M$_\odot$, which is only 40% of the mass found in the single-dish observations of Appleton, Foster, and Davies (1986) and Rots (1980). In fact, RBHAC report that in their lower resolution VLA observations, there is broadly distributed HI between the arms at the level of about 10^{20} cm^{-2} which has been missed in the 8'' map. This interarm emission may not make up

the entire missing flux, but the fact that the total flux is well below the single-dish value indicates that some emission has been resolved out in the 8" map.

We now explore whether these diverse observational results can be explained in the framework of the dissociation model.

i) The HI-CO Offset

First, the fact that the HI arms are, like the Hα arms, offset downstream from the CO arms supports the idea that the HI is produced in star-forming regions. If the HI arms seen in the VLA map simply consisted of gas compressed by the density wave, then we would expect to see the HI emission coincident with the CO emission. However, the fact that in places the HI emission extends upstream from the CO emission implies in the dissociation model that a small fraction of the molecular gas is dissociated by downstream star formation *before* it reaches the zone of peak compression.

ii) The HI Arm Width

We now address the issue of whether the greater width of the HI arms compared to the Hα arms in the inner disk can be explained by a simple "Strömgren sphere" calculation. Certainly the patchiness of the inner HI arms would be expected if each emission feature corresponded to a dissociated region around a young stellar cluster or clusters.

In the Appendix, we calculate the expected sizes of the HII and HI regions along the inner arms of M51 using the observed Hα luminosity of a typical inner-arm

giant HII region to estimate the ionizing photon rate. The effects of dust opacity are included in the calculation by using the HII region extinctions published by van der Hulst *et al.* (1988, hereafter HKCR). With our simple model we predict HII and HI region diameters of 220 and 800 pc, in good agreement with the observed sizes. Therefore, the characteristic size of the HI arms has an explanation in the dissociation picture.

Two perhaps surprising results were found in the calculation presented in the Appendix. First, from the extinction study of HKCR, it is difficult to avoid the conclusion that most of the extinction occurs in dust between the HII regions and the observer, and that therefore there must be large amounts of dust at heights greater than 125 pc (the typical giant HII region radius) above the plane of the galaxy. Then, for any reasonable dust density and distribution, the gas and dust layer in M51 must be substantially thicker than the Galactic layer, having a half-width of about 400 pc. Such a large scale-height could be a consequence of stirring up of the ISM by the enhanced star formation and (presumably) supernova rate on the arms. Higher magnetic and cosmic ray pressures, as a result of star formation or directly due to compression by the strong density wave, could also contribute. However, such a large value is unprecedented, and is not expected given that the velocity dispersion in the HI gas, ~ 10 km s^{-1}, is not as high as one would expect for a gas layer with a 400 pc half-thickness. We therefore view this result with suspicion. Our calculation is, however, not too sensitive to our inferred scale-height. Using a more modest half-thickness of 150 pc, we find an HI region diameter of 600 pc, still in reasonable agreement with observations.

The second surprising result is that we find from two independent methods of estimating the dust surface density that the dust-to-gas ratio (which is a necessary number for calculating the H_2 formation rate) is about equal to the Galactic value. This near equality of dust-to-gas ratios in M51 and the Galaxy may be a cause for concern given that the typical metallicity in the inner disk of M51 is three times the Solar value (Pagel and Edmunds 1981), so that one might expect a higher dust abundance. Using a dust-to-gas ratio of three times the Galactic value gives an HI region diameter of 700 pc.

Our calculation is more sensitive to the gas filling factor than to the above two effects. If the filling factor is less than unity, then our calculated sizes will decrease. For a filling factor of 0.2, the calculated HI diameter is 585 pc, and for 0.1, the diameter is 480 pc. Some of the HI emission features are of this smaller size, but it may be difficult to explain some of the larger emission regions if the filling factor is low.

The H_2 reformation timescale, $n_H(R)^{-1}$, is about $3 \times 10^8 \, \phi$ yr, where ϕ is the filling factor. This timescale can be compared to the time between arm passages, $\pi(\Omega_{rot} - \Omega_P)^{-1}$, to see whether a steady state between dissociation and reformation can be maintained. With the above density wave parameters and rotation curve, the time between arm passages is 5×10^7 yr at 2 kpc from the nucleus, and 2×10^8 yr at 4 kpc. Thus it is plausible that the dissociated gas can reform into molecules before the next arm passage such that a steady state is maintained, provided $\phi \sim 0.1$.

Regardless of variations in the gas parameters discussed above, the important result that the HI regions should be substantially larger than the HII regions is robust for reasonable parameters. However, the Strömgren calculation may not be able to fully explain the characteristic HI arm width, especially if ϕ is as low as 0.1.

Another effect may contribute to the greater HI arm width. Since the hotter stars evolve more rapidly, the ionizing radiation from a stellar cluster will disappear faster than the dissociating radiation, to which B and A stars can contribute significantly. Thus, if young stellar clusters are continuously being formed in the arm, then the zone over which dissociating stars are found will be broader than the zone over which ionizing stars are found. The dissociation zone will also be broader than the typical size of a *single* HI region corresponding to a giant HII region. Some of the HI regions, then, may be due to dissociation by multiple clusters formed at different times on the arms. The width of the zone can be estimated as follows. From simple blackbody approximations, we find that the stars that dominate the dissociating flux are late O and early B stars, which have main sequence lifetimes of $\tau_{MS} \approx 1 - 2 \times 10^7$ yr. The component of circular velocity perpendicular to the arms is approximately $(\Omega_{rot} - \Omega_P) R \sin i$, where i is the pitch angle of the spiral arms, and Ω_P is the pattern speed of the density wave. Tully (1974a) measured i to be 18.5°, and determined a pattern speed, scaled to a distance of 9.6 Mpc, of 38 km s^{-1} kpc^{-1}. The rotation curve is essentially flat at $v_{rot} = 210$ km s^{-1} (Tully 1974b; Scoville and Young 1983). Therefore, at a distance from the nucleus of $R = 3$ kpc, the width perpendicular to the arms of the zone where dissociating stars should be found, assuming that they are all formed at about the same spiral phase, is 0.7 "τ_{MS}

– 13 –

(Myr) $\approx 7 - 13$". Hence the width of the HI arms is likely due in part to this effect. The width expected from this effect is larger near the Inner Lindblad Resonance of the wave and smaller near corotation.

iii) Poor Detailed Spatial Coincidence of HI and HII Regions

It remains to be explained why the detailed spatial coincidence of HII and HI regions is poor, particularly in the inner regions where the existence of the density wave has been established. One possibility, still within the above dissociation scenario, is that some of the HI clouds on the arms are simply regions of low total gas density compared to the typical on-arm density. In terms of the Federman, Glassgold, and Kwan (1979) model, for a given flux of radiation, the HI column density is high in these regions because the molecule formation timescale is relatively long. In other words, G/n is relatively high. However, a visual inspection of Figures 1c and 1d shows that HI regions not associated with Hα emission are sometimes associated with CO emission, and sometimes not, indicating that the HI is not necessarily found in regions of low total gas density.

We prefer the following effects as the more likely reasons for of the lack of correlation. First, as mentioned above, the ionizing radiation from a stellar cluster disappears faster than the dissociating radiation. This effect would not only lead to a lack of correlation but would also explain why some HI regions extend preferentially downstream from the HII regions (Figure 1d). Another possible contributor could be the inevitable supernovae, which will clear out the immediate vicinity of the cluster, where the Hα emission is concentrated, much more effectively than the regions where

the HI is found, much further away from the cluster center. The timescale for this clearing process may be comparable to the age of $\sim 10^7$ yr inferred by Brinks and Bajaja (1986) for the ~ 500 pc diameter HI holes they found in M31. Finally, if some clusters form without many OB stars, they may produce HI regions with little Hα emission.

iv) Interarm HI

The surface density of the smoothly distributed interarm component is 10^{20} cm^{-2}. Such a column density is roughly that expected for a medium consisting of dissociated envelopes of molecular clouds, if the envelopes have a filling factor of order 0.1–0.2 (see Federman, Glassgold, and Kwan 1979). The interarm HI thus has a simple explanation in the dissociation picture. The few interarm clouds seen at 8" resolution do not have much associated Hα emission. They may be dissociation regions around stellar clusters with few OB stars.

III. Infrared Properties

The aim of this analysis is to understand whether or not the infrared emission in M51 arises purely from star-forming regions. Figure 4 shows the *IRAS* maps of M51, while Table 1 lists some of the global properties of the infrared emission. T_W and T_C are the resulting temperatures in a two component fit to the *IRAS* data by Rice *et al.* (1988). T_C is $\lesssim 1\sigma$ above the mean value of all large optical galaxies modelled in this way by Rice *et al.* (1988).

Our first diagnostic is the dimensionless IRE, which is defined as the total IRAS flux (νf_ν summed over the four IRAS bands, although some authors use the 60 and 100 μm bands only) divided by the Lyman continuum flux. Mezger, Smith, and Churchwell (1974) calculate the infrared emission expected from an HII region for a given ionizing photon rate, and show how this photon rate can be estimated from the thermal flux density. The IRE is calculated as follows (Rice et al. 1990):

$$\text{IRE} = 9.4 \ (\text{Hz}^{-1}) \ \frac{F_{IRAS}(10^{-13}\text{Wm}^{-2})}{S_{21}(\text{mJy})} \tag{1}$$

where F_{IRAS} is the total IRAS flux and S_{21} is the thermal continuum flux at 21 cm. The IRE is defined such that a value of unity means that all of the infrared emission can be explained as arising from dust heated by Ly-c photons which have been absorbed and degraded to Lyα by gas. An IRE greater than one implies that some of the infrared emission arises from dust heated directly by photons from H-ionizing stars and from dust heated by stars which provide little ionization. The typical IRE for Galactic HII regions is 6 (Myers et al. 1986). For a galaxy, an IRE well in excess of the value for Galactic HII regions indicates a substantial amount of infrared emission not associated with star-forming regions.

In order to calculate the IRE, we need an estimate of the thermal continuum flux at 21 cm. Thermal-nonthermal flux separations have been carried out independently by Tilanus et al. (1988) and Klein et al. (1984), with both studies finding a thermal flux at 21 cm of about 75 mJy. Thus the IRE of M51 is about 24, which is much higher than the typical value for Galactic HII regions, indicating that

a large fraction of the infrared luminosity originates outside star-forming regions, presumably from the cirrus associated with quiescent molecular clouds and their HI envelopes. The only way to escape this conclusion is to invoke a much higher dust-to-gas ratio in M51, such that in the HII regions of M51, dust grains compete more effectively for ionizing photons than HI atoms relative to Galactic HII regions. However, we show in the Appendix that the dust-to-gas ratio is not significantly different from the Galactic value.

Our second test involves comparing the arm-interarm contrast in the *IRAS* maps with that in our Hα image convolved to the resolutions of the *IRAS* maps. The beam of the *IRAS* detectors is such that the resolution along the in-scan direction (P.A. ≈ 45° for M51) is significantly better than that along the cross-scan direction. The in-scan resolution of the *IRAS* observations is sufficient for the measurement of an arm-interarm contrast at 12, 25 and 60 μm. The in-scan and cross-scan resolutions are listed in Table 2. If all of the infrared emission arises in star-forming regions, we would expect to see the same arm-interarm contrast in the infrared maps as in our Hα image.

Cuts in the in-scan direction of the original 12, 25 and 60 μm maps are presented in Figure 5 along with cuts through Hα and *B*-band images which have been convolved to the *IRAS* resolutions using the elongated *IRAS* beams. Ongoing star formation is traced by the Hα emission while the ISRF is best traced by the *B*-band light. The 100 μm cut is not shown because at the low resolution of the 100 μm data no spiral structure can be seen in either the map or the cut.

Features corresponding to the nuclear region and the outer NE and SW spiral arms can be seen in all of the cuts in Figure 5. The arm-interarm contrast in the 12 μm cut is slightly lower than that at 25 μm. It is clear that the arm-interarm contrast in the *IRAS* cuts in all three bands is lower than in the Hα cuts but higher than in the *B*-band cuts. This result implies that in all three bands there is emission both from dust in star-forming regions and cirrus. For the warm dust (25 and 60 μm) this is not too surprising given the above discussion of the IRE. This result is also understandable for the 12 μm emission if it is dominated by emission from very small grains which are destroyed in star-forming regions.

Deconvolved images of the *IRAS* pointed observations (see Neugebauer *et al.* 1984) of M51 at all four *IRAS* bands were produced at the Infrared Processing and Analysis Center (IPAC) using a Richardson-Lucy deconvolution algorithm (Aumann, H. H., private communication). We examined maps at various stages of the deconvolution procedure and chose ones for the analysis below based on the level of spurious structure introduced in the blank regions around M51 by the deconvolution process. We judged that maps produced using more than 5 iterations at 12 and 25 μm, and 20 iterations at 60 and 100 μm, were possibly unreliable due to this rather subjective criterion. The deconvolved maps using the above numbers of iterations are shown in Figure 6, and the achieved resolutions are listed in Table 2. Cuts were made through these images as before, and are shown in Figure 7, along with Hα and *B*-band cuts at matched resolutions. Increases in the arm-interarm contrast can be clearly seen in the 12, 25 and 60 μm maps, but in the 100 μm map, the companion

is only partially resolved and the outer arms remain unresolved. The 100 μm cut (not shown) shows no evidence for spiral structure.

The smoothness of the 100 μm map and cut is surprising when compared to Smith's (1982) map at 170 μm with 49" resolution (his Figure 2) made with the Kuiper Airborne Observatory. This map, at only slightly better resolution, shows clear spiral structure in the NE and SW. The longer wavelength of his observation should guarantee a smaller contribution to the emission from dust in star-forming regions, since this wavelength traces colder dust, thus reducing the expected contrast relative to that at 100 μm. The likely reason for this discrepancy is that the original 100 μm map had insufficient resolution to detect any spiral structure at all, even in the in-scan direction. Naturally, the deconvolution procedure would not bring out any spiral structure if there were none in the original data.

Figure 7 show the same ordering of cuts by arm-interarm contrast as in Figure 5, and thus point to the same conclusion as that drawn from the original maps: there are at least two components to the infrared emission in the 12, 25 and 60 μm bands.

The deconvolution we have presented is by no means unique. For comparison, we show in Figure 8 a deconvolution of the 60 μm survey data by W. N. Weir (personal communication) using the MEMSYS software (based on the Maximum Entropy Method). This deconvolution method, unlike the Richardson-Lucy algorithm, does not assume that the point-spread function is constant over the field. The achieved resolution, although it almost certainly varies over the map, is obviously much better than that of Figure 6c, and a higher arm-interarm contrast in

the outer arms can be seen. Unfortunately, a comparison of this map with the Hα image would be perilous since the resolution varies over the map. It is therefore not clear how to perform the necessary convolution of the Hα image before the comparison. Compared to the pointed observations, the *IRAS* survey data unfortunately has a worse problem with striping in the in-scan direction, and a stripe can be seen running through the center of M51 in Figure 8 which confuses the interpretation.

We emphasize that our conclusions which are based on differences in arm-interarm contrast between the *IRAS* and Hα images do not depend on the reliability of the Richardson-Lucy deconvolution since the differences can be seen from the cuts through the *original IRAS* maps (Figure 5).

We can make a very rough estimate of the fractions of infrared emission which are associated with star-forming regions and ISRF-heated cirrus. Since the emissivity per dust grain of the cirrus component should be roughly proportional to the ISRF intensity, and since the cirrus arises from dust which is associated with the general gas distribution, the profile of cirrus emission should resemble the product of the *B*-band profile and the profile of total gas surface density. The emission profile of dust in star-forming regions should resemble the Hα profile. For the construction of the total gas profile the resolution of the FCRAO CO map is insufficient. We therefore use the new map of CO emission at 15" resolution from the Nobeyama 45-m and convolve it to the *IRAS* resolutions. Using this simple model and the profiles shown in Figure 5, we estimate that at 60 μm, 75% of the emission comes from the cirrus component, while 25% of the 25 μm emission and 75% of the 12 μm emission

is due to cirrus. For M33, by way of comparison, a more careful decomposition by Rice *et al.* (1990) showed that cirrus accounts for 50% of the 12 and 60 μm emission, and 10% of the 25 μm emission. For both these galaxies then, the 25 μm band contains the highest fraction of emission from star-forming regions.

The results from these two tests imply that a direct interpretation of the *IRAS* luminosity of M51, either the total *IRAS* luminosity or L_{FIR} alone, in terms of a star formation rate, would be spurious. The same conclusion has been reached in studies of many other nearby spirals, where the IRE's range from 13 to 24 (M33 [Rice *et al.* 1990]; M101 [Beichman *et al.* 1987]; and NGC 4565, NGC 891 and NGC 5907 [Wainscoat, de Jong, and Wesselius 1987]). Furthermore, studies of M31 (Walterbos and Schwering 1987) and the Galaxy (Bloemen, Deul, and Thaddeus 1990) have shown that most of the FIR emission arises from cirrus in these galaxies. Finally, Bothun, Lonsdale, and Rice (1989) found for most spiral galaxies in an optically selected sample – using f_{60}/f_{100} as a diagnostic of dust heating sources along with a simple dust-heating model – that dust in star-forming regions and cirrus are both important contributors to the total FIR luminosity.

The position of M51 in the color-color diagram of Helou (1986) confirms the above conclusion. In his Figure 2, M51 lies below the line where half of the infrared emission derives from star-forming regions, implying that the cirrus contributes the majority of the emission.

These results may not be surprising given that the galaxy is very gas-rich. The total mass of gas has been estimated by Scoville and Young (1983) to be 1.2 ×

$10^{10} M_\odot$, of which $9 \times 10^9 M_\odot$ is in molecular form. In comparison, Scoville and Young estimate a dynamical mass of about $10^{11} M_\odot$, so that the gas accounts for fully 13% of the dynamical mass. The high SFR in M51 implies significant dust heating in star-forming regions, but should also imply a relatively intense ISRF, since, for a normal IMF, there will be copious production of intermediate-mass stars which dominate the ISRF. This combination of a rich ISM with an intense ISRF could be the reason for the significant cirrus component.

Throughout this analysis, we have used the term "cirrus" to refer to emission from dust outside of regions of high-mass star formation. It should be noted, however, that Cox, Krügel, and Mezger (1986) conclude that non-ionizing young B and A stars could heat dust in star-forming regions to 30–40 K and provide some of the emission detected by *IRAS* in the Galaxy. It has been suggested for our Galaxy (see Scoville and Sanders 1988), although there is no direct evidence for M51, that B and A star formation is more uniformly distributed than O star formation. If this is the case in M51, then such an infrared emission component from regions of low-mass star formation may have a spatial distribution more like the cirrus component and thus be observationally indistinguishable from cirrus based on the spatial distribution of far infrared (FIR) emission alone. It is therefore worth keeping in mind that radiation from "generally distributed dust" may have more than one origin.

An important consequence of the main conclusion of this section is that infrared emission cannot be used to independently test the hypothesis of density wave triggering of star formation unless the component of emission from star-forming

regions can be effectively isolated, both spatially and spectrally. One should keep in mind that the arms which have been resolved or partially resolved by *IRAS* are beyond the radius of corotation of the density wave and are probably tidal arms generated by the passage of the companion (Tully 1974b; Elmegreen, Elmegreen, and Seiden 1989). Therefore, even the deconvolved *IRAS* images do not begin to resolve the density wave arms and hence cannot be used to test density wave triggering of star formation.

IV. Conclusions

We have used VLA HI data and *IRAS* maps of M51 in an attempt to further understand the consequences of star formation in this molecule-rich galaxy with a strong density wave. From the HI map, we find compelling evidence which favors the idea that the HI is almost entirely a product of dissociation of H_2 in star-forming regions. The radial distribution of HI as well as the characteristic size of the emission features along the arms have simple explanations in the dissociation scenario. The lack of detailed correlation between HI and HII regions has a variety of possible causes. The low-level interarm HI emission can be explained as being due to dissociated envelopes of interarm molecular clouds. There are indications that the gas-to-dust ratio is about equal to the Galactic value. An outstanding issue is the thickness of the gas and dust layer in M51. From the comparison of measured extinctions with models one infers that the layer is substantially thicker than that of the Galaxy. However, the large gas dispersions expected in such a case are not seen

and there is no direct evidence to support this result. The issue deserves further attention.

The IRE and the reduced arm-interarm contrast of the *IRAS* maps compared to the Hα image both indicate that a substantial fraction of the infrared emission detected by *IRAS* does not arise in star-forming regions, but rather from dust associated with generally distributed gas. Given the high surface density of gas in M51, this result is perhaps not too surprising. The same conclusion has now been drawn for several nearby galaxies. An important implication of this result is that it will be difficult to interpret the FIR emission from M51 in terms of recent star formation, and thus to use FIR emission to check the hypothesis of density wave triggering of star formation. Regardless of whether a reliable separation of emission components can be done, the resolution of the *IRAS* maps is insufficient to resolve the inner, density-wave spiral arms.

Acknowledgements

Appendix

We show here through a "Strömgren" analysis that the large observed sizes of the discrete HI regions along the inner arms can be understood if they owe their existence to photo-dissociation by the OB associations along the arms.

A typical HII region on the inner arms has an extinction-corrected Hα luminosity of 5×10^{39} erg s^{-1} (HKCR), which corresponds to about 3.5×10^{51} ionizing photons per second, or 70 O5 stars (Kennicutt, Edgar, and Hodge 1989). We assume that all photons shortward of 13.6 eV are absorbed by H atoms, while photons with energies between 11.2 and 13.6 eV are available to dissociate H$_2$ molecules. We ignore heavy elements for the moment; however we do allow for dust opacity.

At any radius r within an HII region, we have the following balance between ionization and recombination:

$$\frac{Q}{4\pi r^2} n_{HI} \bar{a}_{HI} e^{-(\bar{\tau}_D(r) + \bar{\tau}_{HI}(r))} = n_e^2 \alpha_B \qquad (A1)$$

where Q is the ionizing photon rate, n_{HI} is the atomic H density, $\bar{a}_{HI}$ is the atomic absorption coefficient, averaged over frequencies above the ionization threshold, $\bar{\tau}_D(r)$ and $\bar{\tau}_{HI}(r)$) are the frequency-averaged dust and atomic H opacities at radius r, n_e is the electron density, and α_B is the appropriate recombination coefficient in the "on-the-spot" approximation.

For the HI case, we assume that all photons with 11.2 eV $< E <$ 13.6 eV are available for the dissociation of H$_2$. Using simple blackbody approximations and a

Salpeter Initial Mass Function, we estimate that the photon rate in the above energy range for a stellar cluster is about 50% of the ionizing photon rate. We use this ratio for the HII regions of M51. Only about 10% of absorptions of such photons lead to a dissociation (Spitzer 1978, p. 100), so a factor of 0.1 must be included in the usual Strömgren calculation to account for this. Thus we have

$$\frac{Q}{80\pi r^2} n(H_2)\bar{a}_{H_2} e^{-(\tau_D(r)+\tau_{H_2}(r))} = R n_H n(HI) \qquad (A2)$$

where $n(H_2)$ is the molecular density, $\bar{a}_{H_2}$ is the molecular absorption coefficient averaged over the above energy range, $\bar{\tau}_D(r)$ and $\bar{\tau}_{H_2}(r)$ are the dust and H_2 opacities at radius r averaged over the above energy range, n_H is the total density of H and $n(HI)$ is the density of atomic H. R is the H_2 formation constant (Spitzer 1978, p. 123), which is proportional to the projected area of dust grains per H nucleus, so that it must be scaled from the Galactic value of $R_{Gal} = 3.0 \times 10^{-17}$ cm^3 s^{-1} by the estimated dust-to-gas ratio contrast between M51 and our Galaxy (assuming similar grain properties). So equation A2 becomes

$$\frac{Q}{80\pi r^2} n(H_2)\bar{a}_{H_2} e^{-(\tau_D(r)+\tau_{H_2}(r))} = R_{Gal}\frac{D_{M51}}{D_{Gal}} n_H n(HI) \qquad (A3)$$

where D_{M51} and D_{Gal} are the dust-to-gas ratios in M51 and the Galaxy.

The electron density can be estimated from the HII region study of HKCR. They used a 6-cm VLA map with a resolution of 8", and an Hα image smoothed to the same resolution to estimate HII region projected areas and mean densities.

Using their measured diameters of about 10" from their smoothed image, they found a typical density of 1.5 cm^{-3}. Since the actual measured diameter of the typical HII region in our image is 5.5", the projected areas determined by HKCR are too large, and the density must therefore be scaled up by the correct projected area, giving $n_e = 5$ cm^{-3}. This density is typical of extragalactic giant HII regions (Kennicutt 1984).

The extinction in the HI and HII regions can also be estimated from HKCR. From a comparison of the extinction at Hβ and the Hα-Hβ color excess with the models of Caplan and Deharveng (1986) for 11 giant HII regions , they deduce that only about 0.5 mag of the typical 1.8 mag of visual extinction could arise from within the HII regions, and that the remaining extinction occurs in foreground dust. A model with most of the extinction occurring in the HII regions appears to be strongly ruled out by their data. Assuming spherical symmetry for the HII regions, one therefore requires most of the dust to be at heights above $\sim$125 pc, which is the radius of a typical giant HII region. It would therefore seem likely that, if the dust density above the HII regions is not too different from that inside the HII regions, the dust layer half-thickness is perhaps 3 − 4 times the typical giant HII region radius, or $\sim$ 450 pc. Alternatively, one can assume spherical symmetry for the HI regions and again infer that the gas, and presumably the dust, extends to about 400 pc above the plane. This issue is discussed further in the main part of the text since this scale-height is unusually large. We adopt, then, a total A_V of 0.5 mag in the HII region, and 1.8 mag in the HI region. We use the Galactic

extinction curve from Spitzer (1978, p. 158) to convert these to extinctions at 1000 Å.

The dust-to-gas ratio can simply be estimated from the typical HII region visual extinction of about 1.8 mag and the mean gas surface density at 3 kpc from the nucleus of 100 $M_\odot$ pc^{-2} (Lord and Young 1990). This extinction represents the contribution from the HII region and the dust layer above it. There should therefore be an additional 1.3 mag of extinction from the dust associated with the gas layer on the opposite side of the plane, leading to a total extinction of 3.1 mag. Assuming the gas and dust are coextensive, these numbers imply a column density of 2.1×10^{21} cm^{-2} per magnitude of visual extinction, compared to the Galactic value of 2×10^{21} cm^{-2} (Spitzer 1978, p. 156, 161). The inferred dust-to-gas ratio is thus about equal to the Galactic value. A check on this number can be obtained from Smith's (1982) estimate of the dust mass surface density in the inner disk of M51 (Smith's "Bar" region) of 0.64 $M_\odot$ pc^{-2}. The dust-to-gas mass ratio calculated in this way is thus 0.006, again about equal to the Galactic value.

For n_H, we use the above H$_2$ surface density and find $n_H = 4$ cm^{-3}. For n(HI), we estimate a value of 0.5 cm^{-3} on the arms from the VLA map. Both numbers assume the above half-thickness of the gas layer of 450 pc.

Equations A2 and A3 are easily solved for the ratio of the Strömgren radius in the presence of dust to the dust-free Strömgren radius by the method described in Spitzer (1978, p. 111-113). Since we used the observed sizes to calculate the dust opacity, our solution must reproduce these sizes in order to be self-consistent. In

fact, we derive diameters of 220 and 800 pc for the HII and HI regions, in good agreement with observations.

Of the most abundant heavy elements, He, N and O will not compete with H_2 for the dissociating photons since their ionization potentials are above 13.6 eV. Only CI has an ionization potential (11.3 eV) in the relevant energy range. We show here, however, that we do not expect CI to compete with HI for this spectral range of photons. In equilibrium, the absorption rate by H_2 molecules will equal 10 times the formation rate, or 3.5×10^{-16} cm^{-3} s^{-1}. In contrast, essentially all absorptions by CI in this energy range will lead to ionization, and by balancing ionizations with recombinations, using a heavy element abundance of 3 times Solar (Pagel and Edmunds 1981), we find a photon absorption rate equal to 2.5×10^{-17} cm^{-3} s^{-1}. Therefore, our results should not be affected by the presence of CI. Including depletion into dust and molecules would strengthen this conclusion.

Table 1. Infrared Properties of M51

		Reference
$f_\nu(12\ \mu m)$	11 ± 5 Jy	Rice *et al.* 1988
$f_\nu(25\ \mu m)$	17 ± 6 Jy	"
$f_\nu(60\ \mu m)$	109 ± 4 Jy	"
$f_\nu(100\ \mu m)$	292 ± 7 Jy	"
$f_\nu(170\ \mu m)$	393 Jy	Smith 1982
L_{FIR} (40 μm–120 μm)	$1.9 \times 10^{10}\ L_\odot$	Rice *et al.* 1988
L_{FIR}/L_B	0.7	"
L_{IRAS} (5 μm–1 mm)	$5.0 \times 10^{10}\ L_\odot$	"
Infrared Excess (IRE)	24	This work
T_W	209.4 K	Rice *et al.* 1988
T_C	33.4 K	Rice *et al.* 1988

Table 2. Original and Deconvolved *IRAS* Map Resolutions

Band	Original Resolution In-Scan/Cross-Scan FWHM	Deconvolved Resolution In-Scan/Cross-Scan FHWM
12 μm	45"/271"	30"/78"
25 μm	43"/271"	32"/81"
60 μm	83"/278"	33"/56"
100 μm	170"/290"	59"/69"

References

Allen, R. J., Atherton, P. D., and Tilanus, R. P. J. 1986. *Nature*, **319**, 296.

Appleton, P. N., Foster, P. A., and Davies, R. D. 1986. *M. N. R. A. S.*, **221**, 393.

Beichman, C., Boulanger, F., Rice, W., and Lonsdale Persson, C. J. 1987, in *Star Formation in Galaxies*, ed. C. J. Lonsdale Persson (NASA: CP 2466), p. 297.

Bloemen, H., Deul, E. R., and Thaddeus, P. 1990. preprint.

Bothun, G. D., Lonsdale, C. J., and Rice, W. 1989. *Ap. J.*, **341**, 129.

Brinks, E. and Bajaja, E. 1986, *Astr. Ap.*, **169**. 14.

Caplan, J. and Deharveng, L. 1986, *Astr. Ap.*, **155**. 297.

Cox, P., Krügel, E., and Mezger, P. G. 1986, *Astr. Ap.*, **155**, 380.

Cox, P. and Mezger, P. G. 1987, in *Star Formation in Galaxies*, ed. C. J. Lonsdale Persson (NASA: CP 2466), p. 23.

Elmegreen, B. G., Elmegreen, D. M. and Seiden, P. E. 1989, *Ap. J.*, **343**, 602.

Federman, S. R., Glassgold, A. E., and Kwan, J. 1979, *Ap. J.*, **227**, 466.

Helou, G. 1986, *Ap. J. (Letters)*, **311**, L33.

Hollenbach, D., Werner, M. W., and Salpeter, E. E. 1971, *Ap. J.*, **163**, 155.

Kennicutt, R. C. 1984, *Ap. J.*, **287**, 116.

Kennicutt, R. C., Edger, B. K., and Hodge, P. W. 1989, *Ap. J.*, **339**, 761.

Klein, U., Wielebinski, R., and Beck, R. 1984, *Astr. Ap.*, **135**, 213.

Lonsdale-Persson, C. J. and Helou, G. 1987, in *Star Formation in Galaxies*, ed. C. J. Lonsdale Persson (NASA: CP 2466), p. 23.

Low, F. J. *et al.* 1984, *Ap. J. (Letters)*, **278**, L19.

Lord, S. D., and Young, J. S. 1990, *Ap. J.*, **356**, 135.

Mezger, P. G. 1978, *Astr. Ap.*, **70**, 565.

Mezger, P. G., Smith, L. F., and Churchwell, E. 1974, *Astr. Ap.*, **32**, 269.

Myers, P. C., Dame, T. M., Thaddues, P., Cohen, R. S., Silverberg, R. F., Dwek, E., and Hauser, M. G. 1986, *Ap. J.*, **301**, 398.

Neugebauer, G. *et al.* 1984, *Ap. J. (Letters)*, **278**, L1.

Pagel, B. E. J., and Edmunds, M. G. 1981, *Ann. Rev. Astr. Ap.*, **19**, 77.

Puget, J. L., Léger, A., and Boulanger, F. 1985, *Astr. Ap.*, **142**, L19.

Rand, R. J., and Kulkarni, S. R. 1990a, *Ap. J. (Letters)*, **349**, L43 (RK).

Rand, R. J., and Kulkarni, S. R. 1990b, in preparation.

Rand, R. J. and Tilanus, R. P. J. 1990, in *The Interstellar Medium in Galaxies*, eds. H. A. Thronson and J. M. Shull (Dordrecht:Kluwer), p. 525.

Rice, W., Boulanger, F., Viallefond, F., Soifer, B. T., and Freedman, W. L. 1990, *Ap. J.*, **358**, 418.

Rice, W., Lonsdale, C. J., Soifer, B. T., Neugebauer, G., Kopan, E. L., Lloyd, L. A., De Jong, T., and Habing, H. J. 1988, *Ap. J. Suppl.*, **68**, 91.

Rots, A. H. 1980, *Ap. J. Suppl.*, 41, 189.

Rots, A. H., Bosma, A., van der Hulst, J. M., Athanassoula, E., and Crane, P. C. 1990, *A. J.*, 100, 387 (RBHAC).

Sandage, A., and Tammann, G. A. 1975, *Ap. J.*, 196, 313.

Scoville, N. Z., and Sanders, D. B. 1986, in *Interstellar Processes*, ed. D. Hollenbach and A. Thronson (Dordrecht: Reidel), p. 21.

Scoville, N. Z., and Young, J. S. 1983, *Ap. J.*, 265, 148.

Smith, J. 1982, *Ap. J.*, 261, 463..

Spitzer, L. J. 1978, *Physical Processes in the Interstellar Medium* (Wiley, New York, NY.)

Tilanus, R. P. J., and Allen, R. J. 1989;Ap. J. (Letters);339;L57 (TA)

Tilanus, R. P. J., Allen, R. J., van der Hulst, J. M., Crane, P. C., and Kennicutt, R. C. 1988, *Ap. J.*, 330, 667.

Tully, R. B. 1974a, *Ap. J. Suppl.*, 27, 437.

Tully, R. B. 1974b, *Ap. J. Suppl.*, 27, 449.

van der Hulst, J. M., Kennicutt., R. C., Crane, P. C., and Rots, A. H. 1980, *Astr. Ap.*, 195, 38 (HKCR).

Vogel, S. N., Kulkarni, S. R., and Scoville, N. Z. 1988, *Nature*, 334, 402 (VKS).

Wainscoat, R. J., de Jong, T., and Wesselius, P. R. 1987, *Astr. Ap.*, 181, 225.

Walterbos, R. A. M. and Schwering, P. B. W. 1987, *Astr. Ap.*, 180, 27.

Figure Captions

FIG. 1. Shown in the top left panel are contours of CO emission from the OVRO mosaic overlaid on a red CCD image. The contour levels are as stated in RK. The top right panel shows CO contours overlaid on an Hα CCD image. The bottom left panel shows contours of CO overlaid on a grey-scale representation of the VLA 21-cm map. The bottom right panel shows contours of 21-cm emission on the Hα image. The contour levels are 1, 1.5, 2, and 4 times 8.4×10^{20} cm^{-2} in the bottom right panel.

FIG. 2. The radial distributions of total gas surface density, Hα emission, and HI surface density.

FIG. 3. A close-up of a spiral arm segment south of the nucleus showing the small scale relationship between HI, Hα and CO emission. The solid contours are HI emission. The levels are 1, 2, 3, 4, and 5 times 8.4×10^{20} cm^{-2}. The dashed contours are CO emission from the OVRO mosaic. The grey-scale represents Hα emission. The flow direction is indicated. The area labelled "A" is an example of a region where an HI peak coincides with an HII region. The areas labelled "B" are examples of HI peaks *between* HII regions.

FIG. 4. The original maps of *IRAS* emission in M51: a) 12μm, b) 25μm, c) 60μm, and d) 100μm. The unit contour interval is the estimated noise in the map.

FIG. 5. Cuts through the original *IRAS* maps and Hα and *B*-band CCD images along the *IRAS* in-scan direction from NE to SW.

FIG. 6. The deconvolved maps of *IRAS* emission in M51: *a)* 12μm, *b)* 25μm, *c)* 60μm, and *d)* 100μm. The unit contour interval is the estimated noise in the map.

FIG. 7. Cuts through the deconvolved *IRAS* maps and Hα and *B*-band CCD images along the *IRAS* in-scan direction from NE to SW.

FIG 8. Deconvolution of the *IRAS* 60μm survey data on M51 by W. N. Weir using the MEMSYS package. The contour levels are 5, 10, 15, 20, 25, 30, 35, 40, 50, 60, 70, 80, and 90 percent of the peak.

Postal Addresses

Shrinivas R. Kulkarni and Richard J. Rand

Division of Physics, Math and Astronomy

California Institute of Technology

105-24

Pasadena, CA 91125

W. Rice

Infrared Processing and Analysis Center

California Institute of Technology

100-22

Pasadena, CA 91125

M51

CO on Red Continuum

CO on Hα

CO on HI

HI on Hα

Fig 2

DECLINATION

RIGHT ASCENSION

47 26 45

25 45   30   15   00   30

13 27 52   50   48   46   44
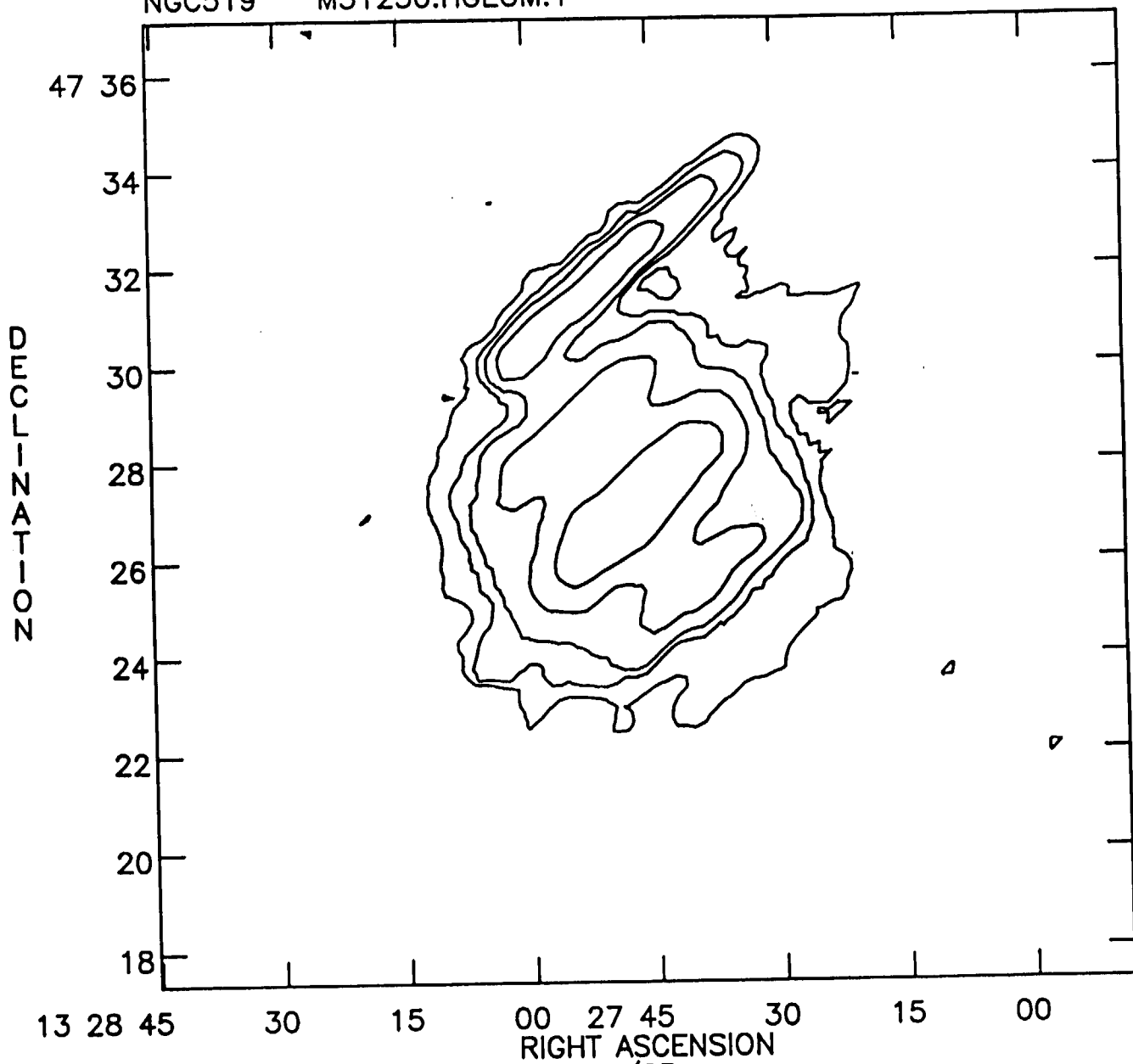
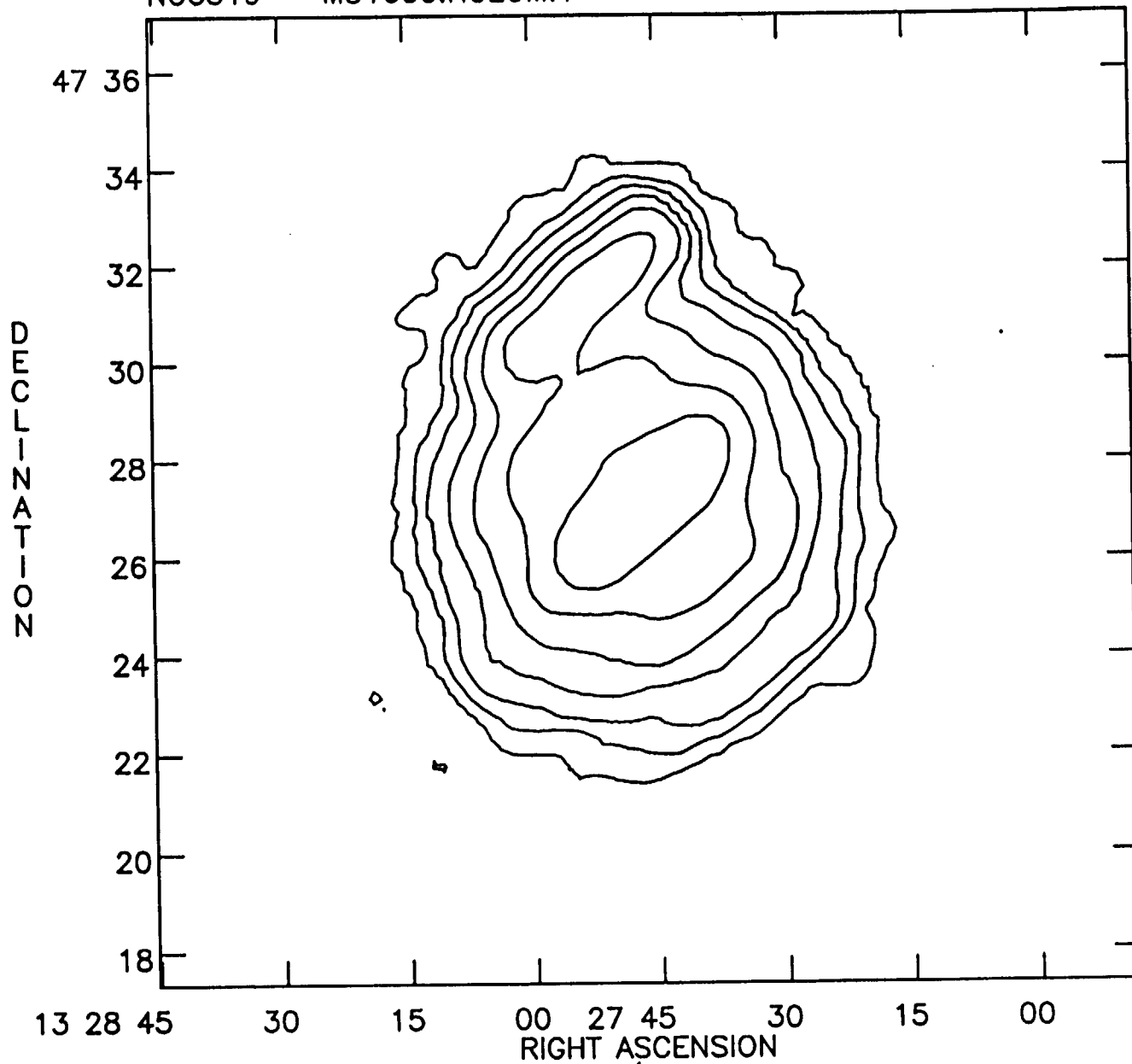Fig 4a
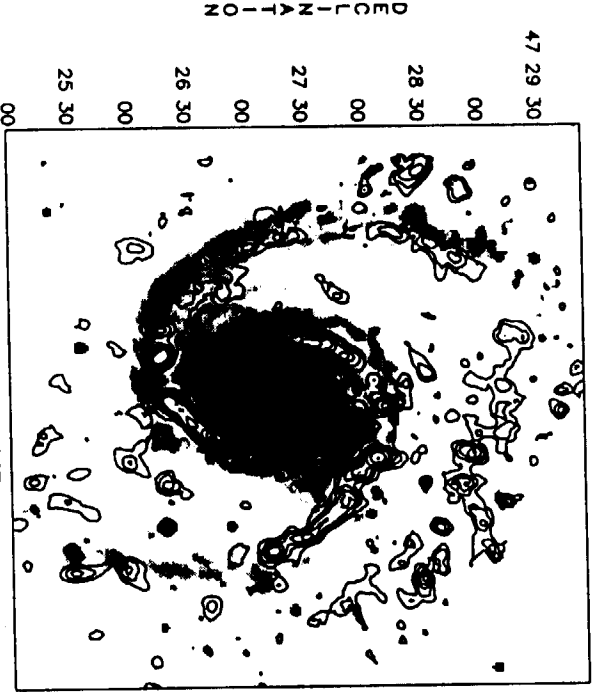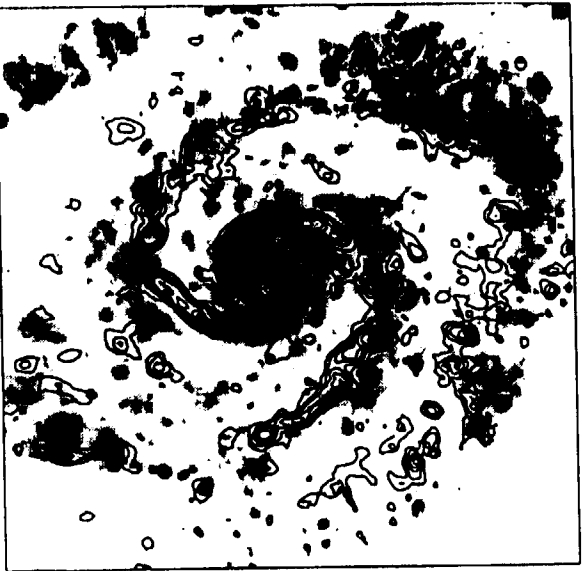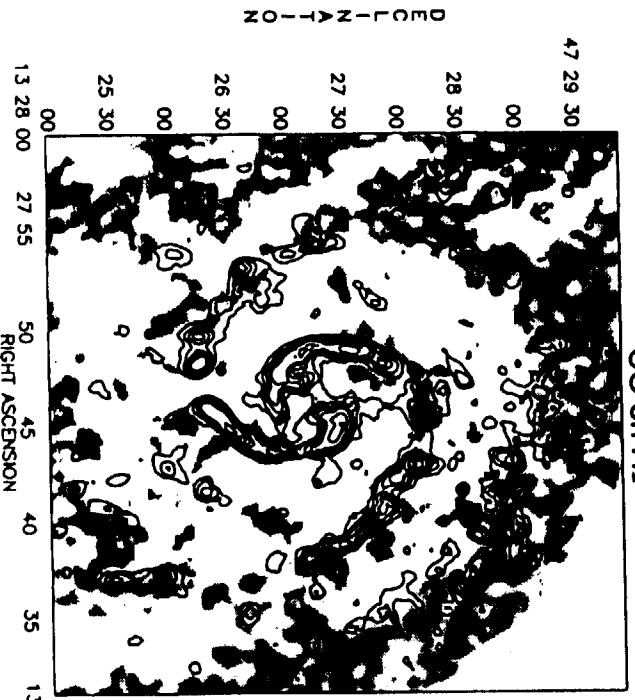
NGC519   M51120.HGEOM.1
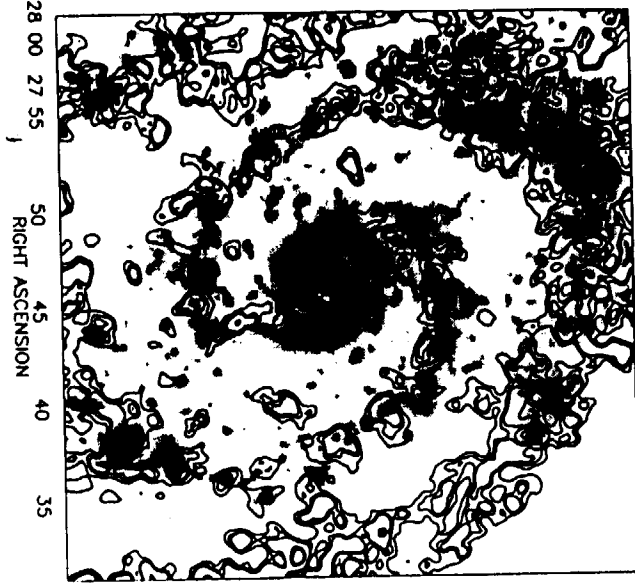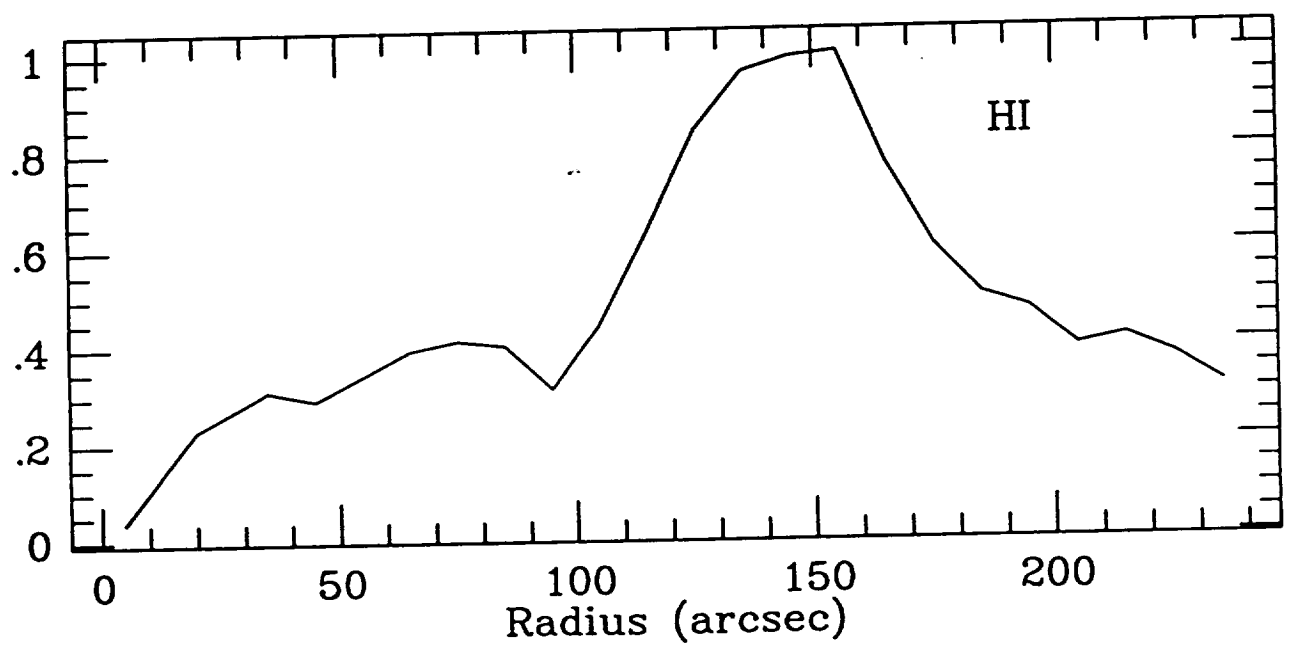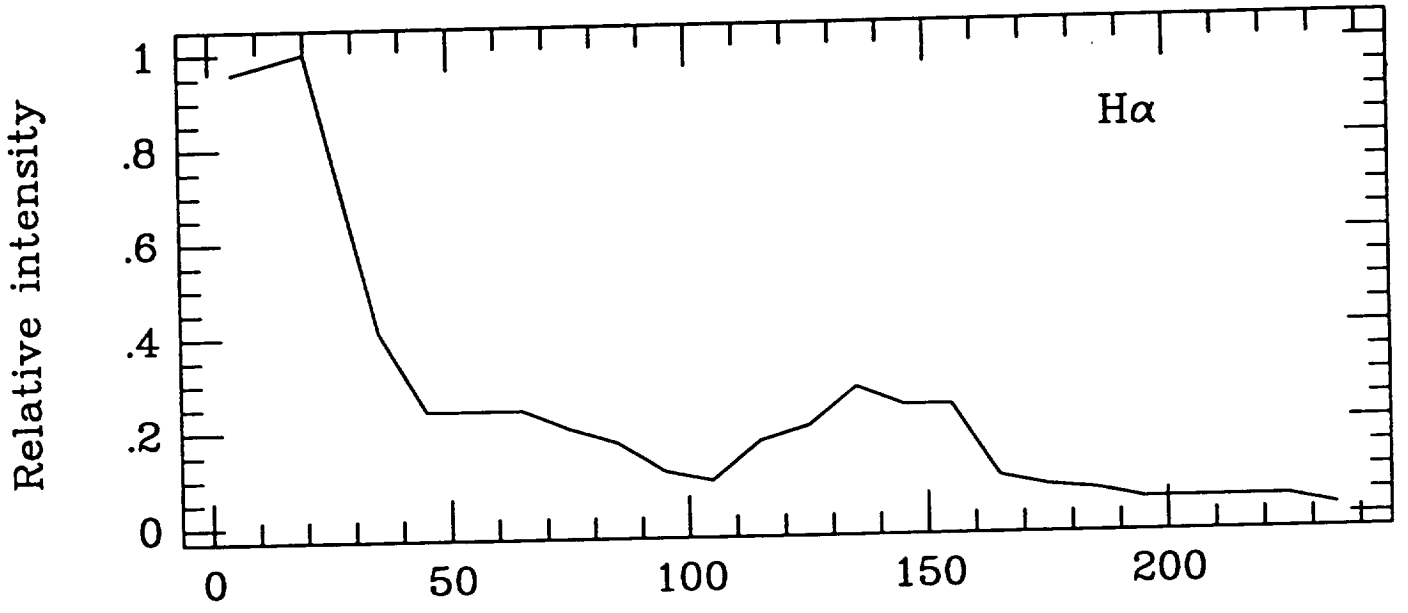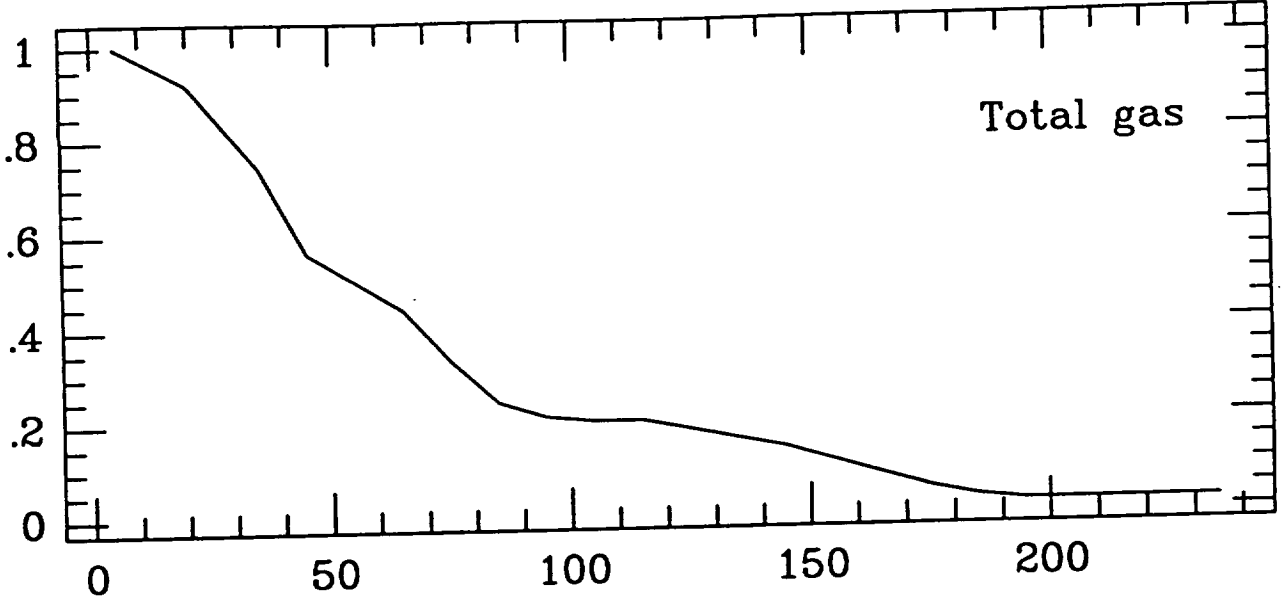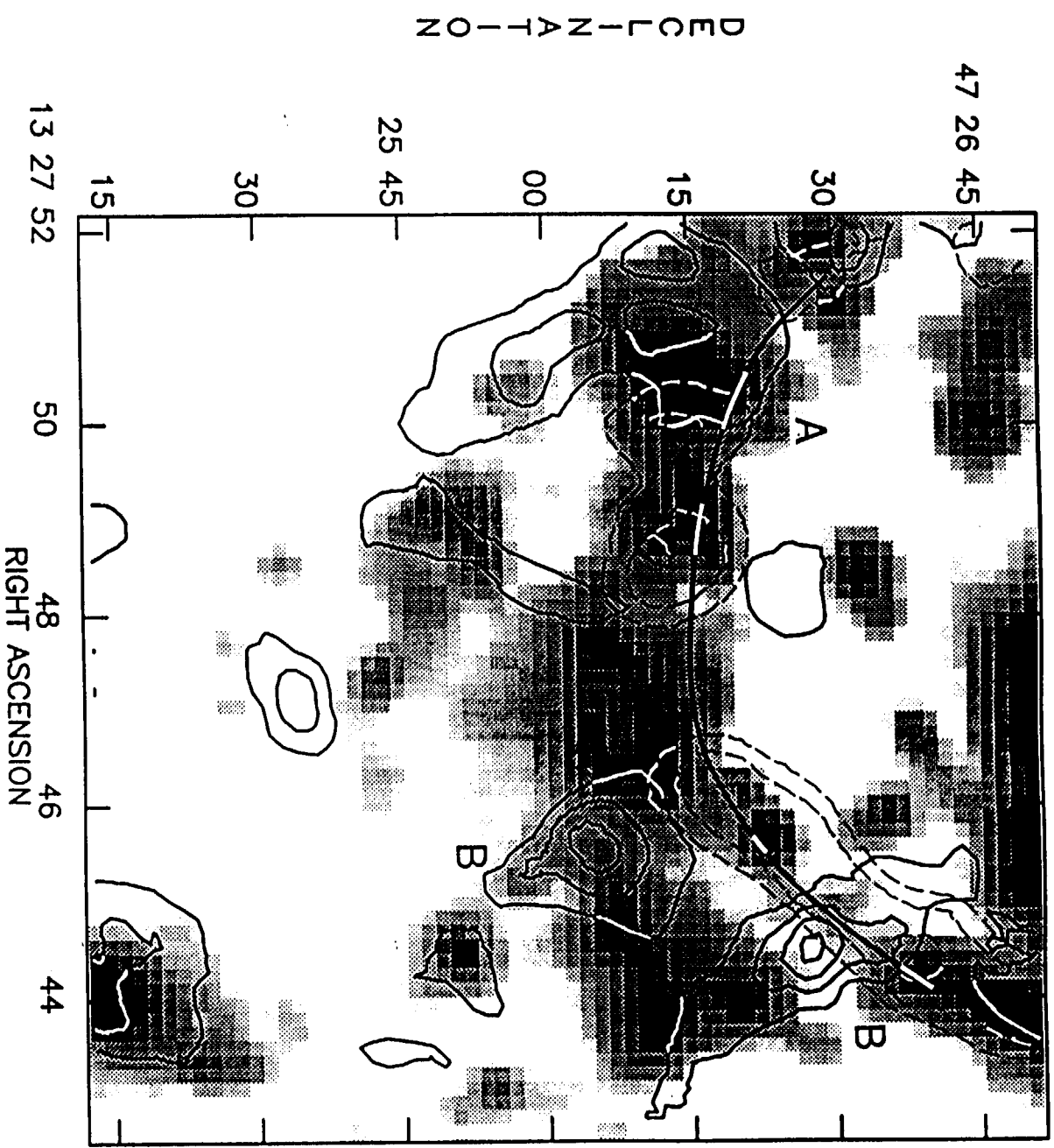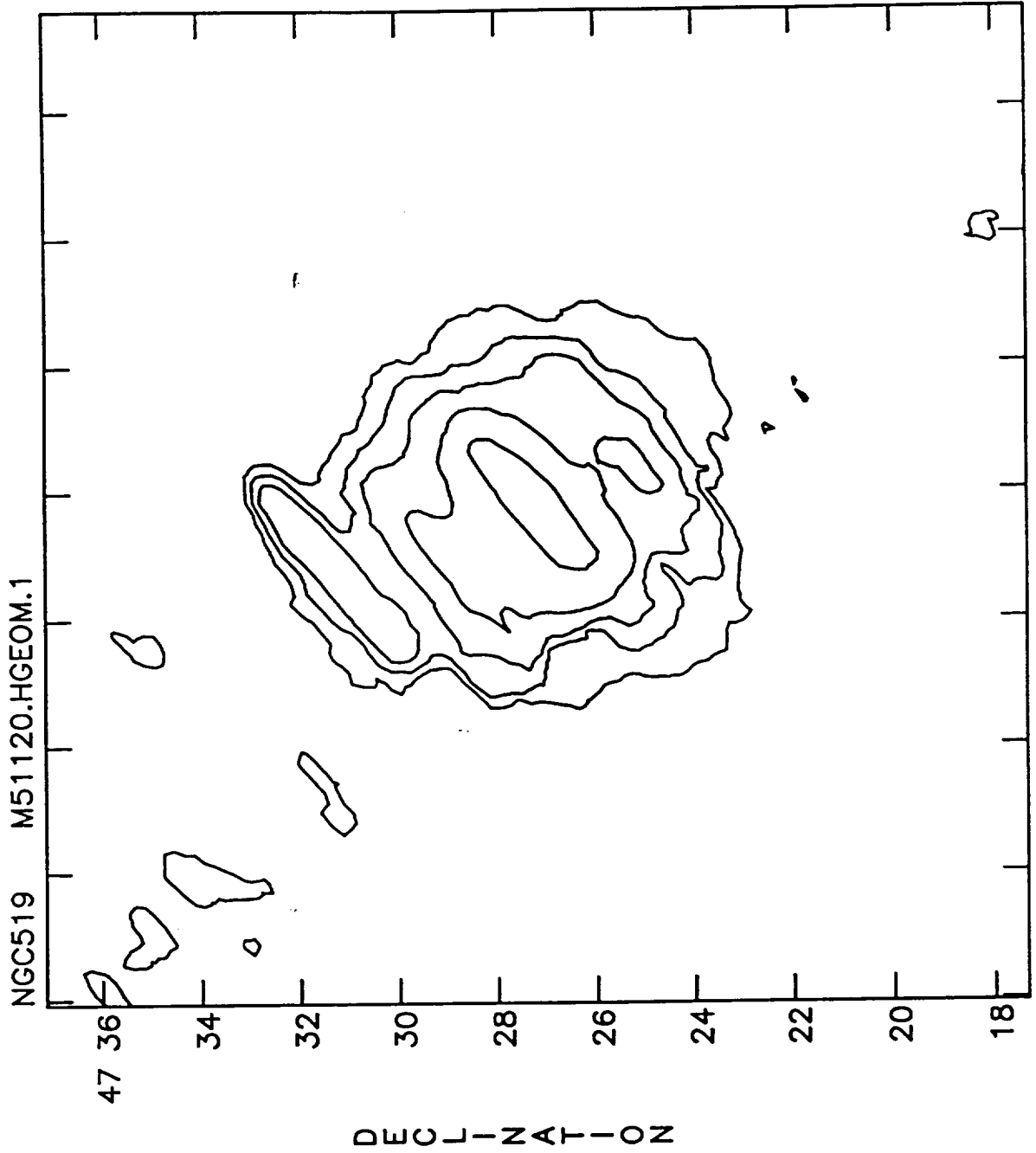
Peak flux = 8.3567E+00 MJY/SR
Levs = 1.6559E-01 * (3.000, 6.000, 10.00,
20.00, 40.00)

RIGHT ASCENSION

NGC519   M51250.HGEOM.1

Peak flux = 1.2654E+01 MJY/SR
Levs = 1.7925E-01 * (3.000, 6.000, 10.00,
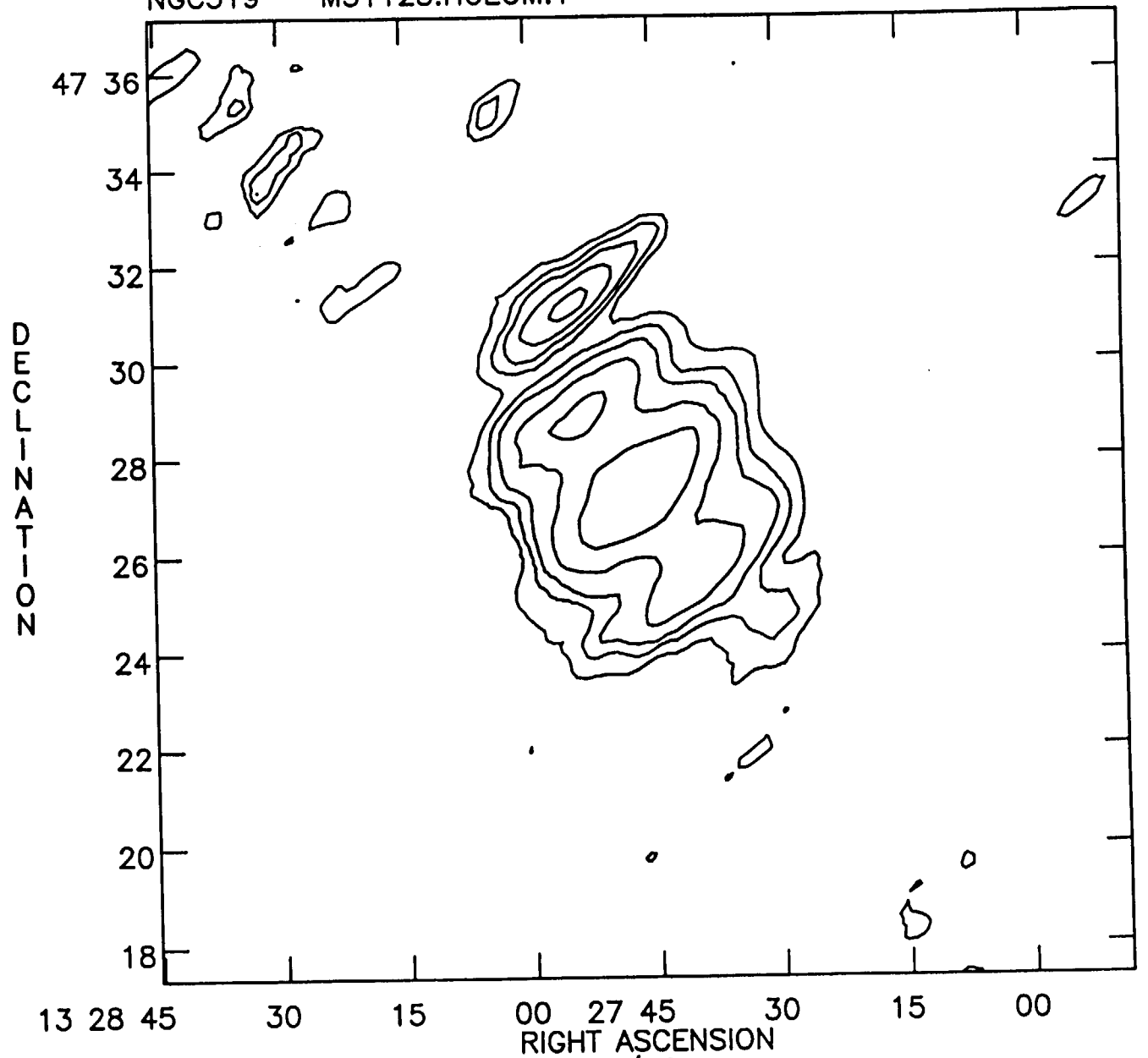20.00, 40.00)

NGC519   M51600.HGEOM.1

DECLINATION

47 36

34

32

30

28

26

24

22

20

18

RIGHT ASCENSION

13 28 45   30   15   00 27 45   30   15   00

Peak flux =   7.5712E+01 MJY/SR
Levs =   2.5147E−01 * (3.000, 6.000, 10.00,
 20.00, 40.00, 80.00, 160.0)

NGC519   M511000.HGEOM.1
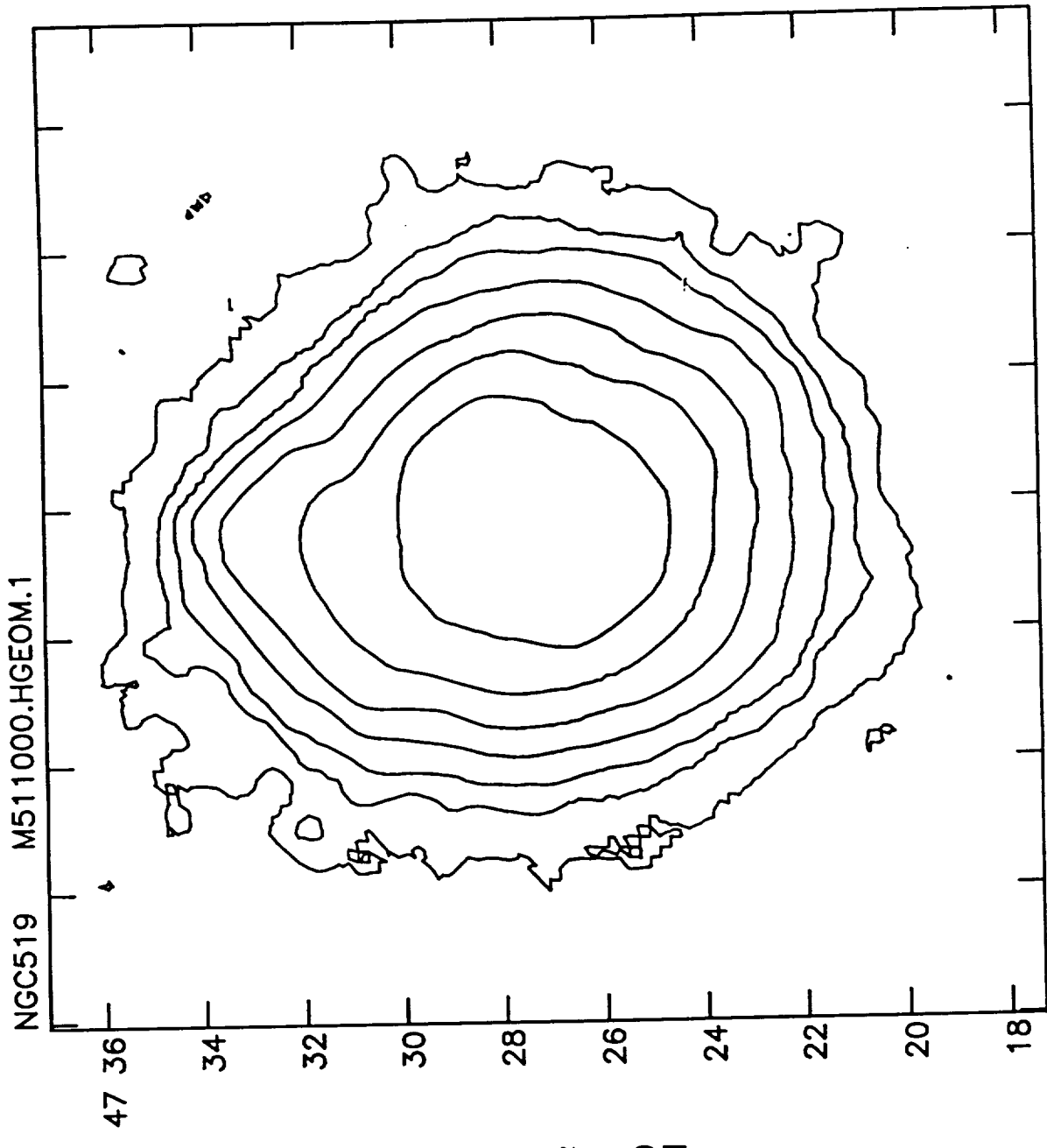
Peak flux = 1.1836E+02 MJY/SR
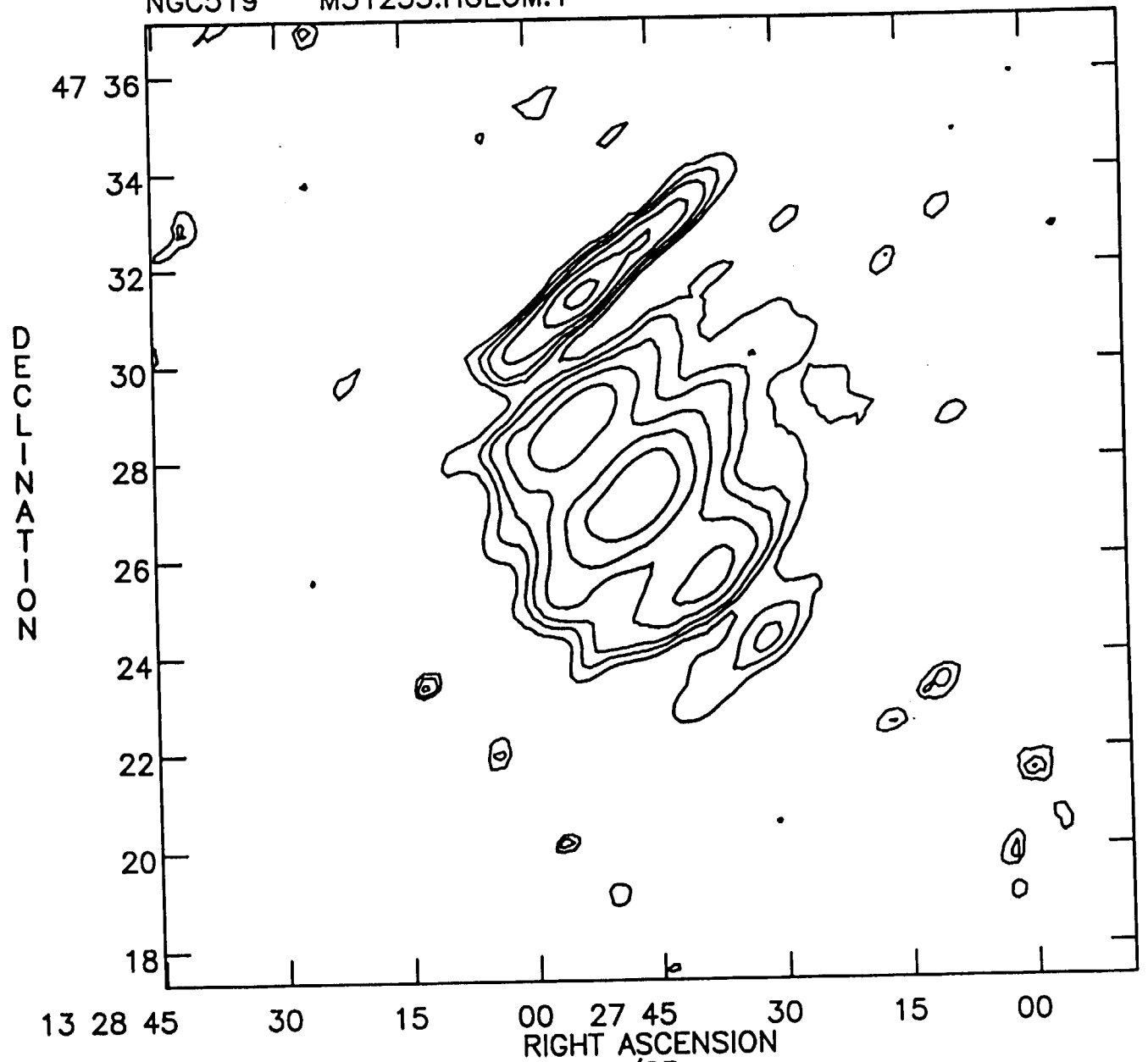Levs = 3.6593E-01 * (3.000, 6.000, 10.00,
20.00, 40.00, 80.00, 160.0)

RIGHT ASCENSION

DECLINATION

IRAS 12μm ——
Hα ——
Blue - - -

IRAS 25μm ——
Hα ——
Blue - - -

IRAS 60μm ——
Hα ——
Blue - - -

Normalized intensity

Offset from nucleus (arcmin)

NGC519   M51125.HGEOM.1

Peak flux =   1.6243E+01 MJY/SR
Levs = 1.6559E-01 * (3.000, 6.000, 10.00,
 20.00, 40.00)

NGC519   M51255.HGEOM.1

DECLINATION

47 36

34

32

30

28

26

24

22

20

18
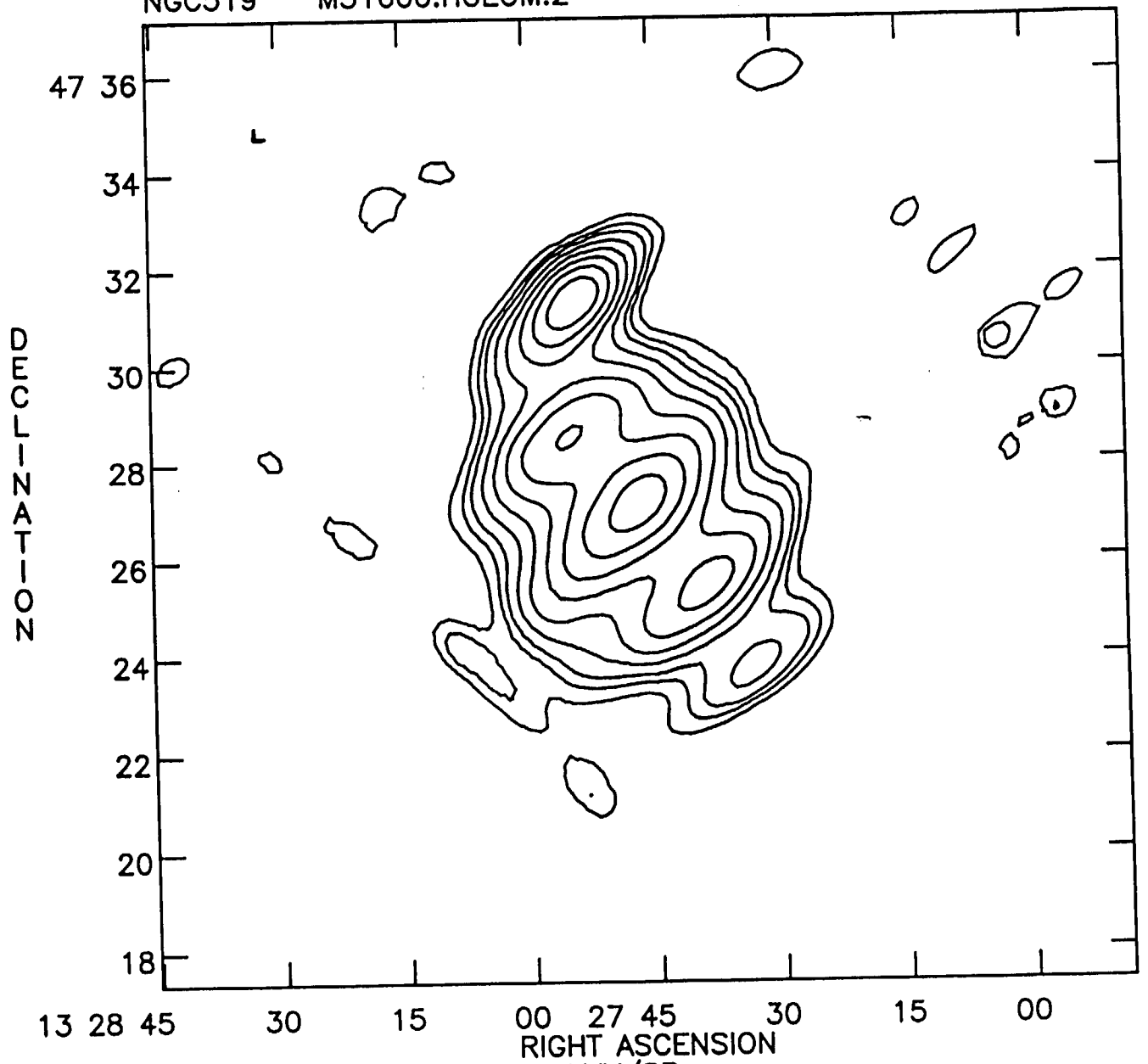
13 28 45   30   15   00   27 45   30   15   00
RIGHT ASCENSION

Peak flux =   2.8520E+01 MJY/SR
Levs =   1.7925E-01 * (3.000, 6.000, 10.00,
20.00, 40.00, 80.00)
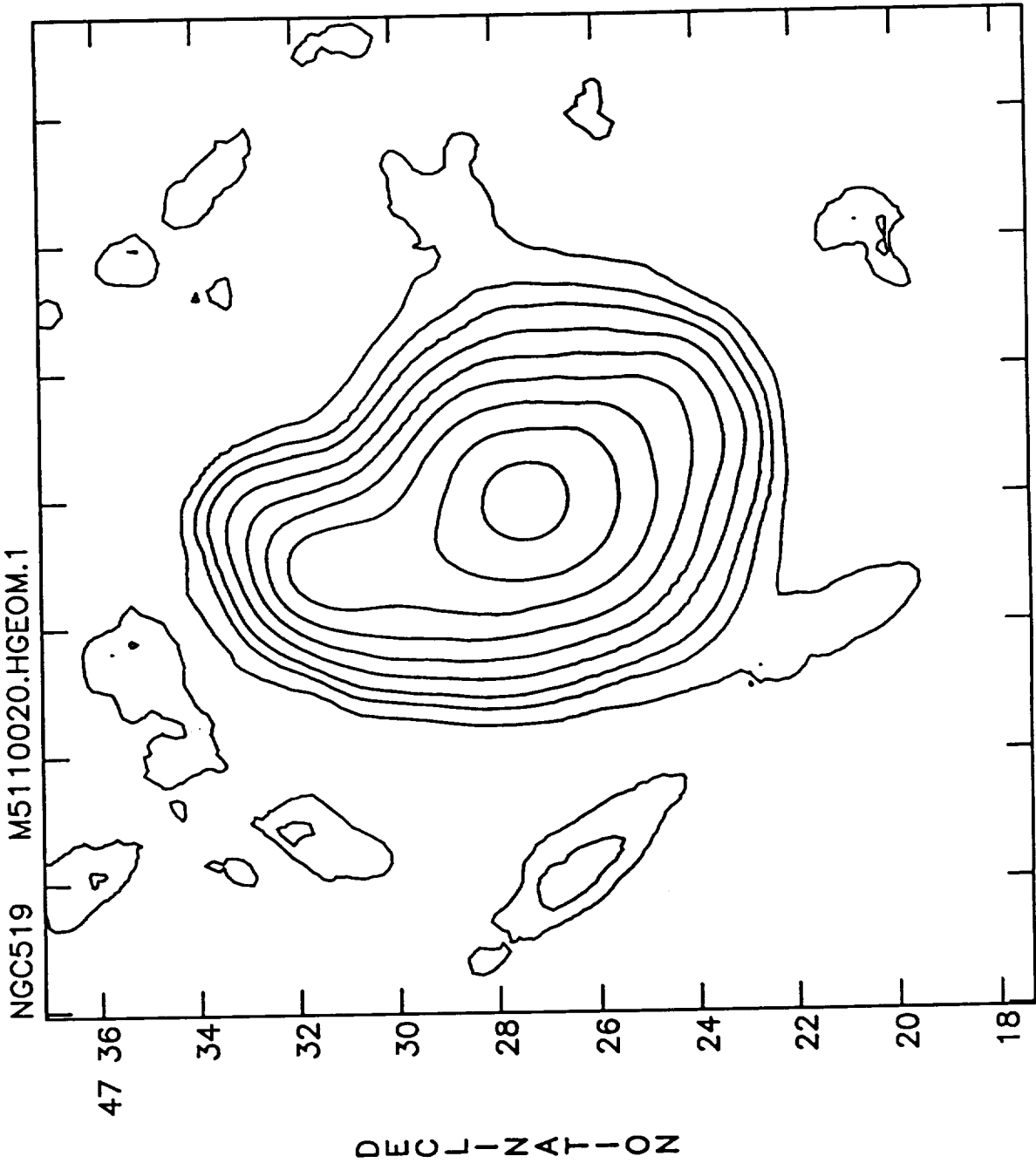
NGC519   M51600.HGEOM.2

Peak flux = 2.4053E+02 MJY/SR
Levs = 2.5147E-01 * (3.000, 6.000, 10.00,
20.00, 40.00, 80.00, 160.0, 320.0, 640.0)

NGC519   M5110020.HGEOM.1

DECLINATION

47 36
34
32
30
28
26
24
22
20
13 28 45

00   15   30   00 27 45   30   15   00
RIGHT ASCENSION

Peak flux = 3.0874E+02 MJY/SR
Levs = 3.6593E-01 * (3.000, 6.000, 10.00,
20.00, 40.00, 80.00, 160.0, 320.0, 640.0)

Normalized intensity

Offset from nucleus (arcmin)

IRAS 12μm
Hα
Blue

IRAS 25μm
Hα
Blue

IRAS 60μm
Hα
Blue

Fig 7

Fig 8

R. A. Offset (arcmin)

Dec. Offset (arcmin)